Synthesis of Polymer-Stabilized Nanosized Rhodium Particles in the Interlayer Space of Layered Silicates

Szilvia Papp,[†] József Szél,[‡] Albert Oszkó,[§] and Imre Dékány*[,†,‡]

Nanostructured Materials Research Group of the Hungarian Academy of Science, Department of Colloid Chemistry, and Department of Solid State and Radiochemistry, University of Szeged, H-6720 Szeged, Aradi v. t. 1, Hungary

Received April 7, 2003. Revised Manuscript Received November 6, 2003

Rhodium nanoparticles were prepared by homogeneous nucleation in aqueous polymer solution and by heterogeneous nucleation on the interlayer space of layered montmorillonite and kaolinite minerals by reduction with $NaBH_4$ in aquatic dispersion. Rhodium particles were stabilized by polymers and by the lamellae of layered silicates. The effect of the molecular mass and the concentration of polymers on the size of the particles formed was studied using neutral polyvinylpyrrolidone, cationic poly(diallyldimethylammonium chloride), and anionic poly(sodium 4-styrenesulfonate). The effect of the concentration of the rhodium precursor was also examined; reduction of rhodium ions was controlled by X-ray photoelectron spectroscopy. Interlamellar incorporation of nanoparticles was monitored by X-ray diffraction and small-angle X-ray scattering verified by transmission electron microscopy. Average particle size fell within the range of 1−3 nm, depending on the stabilization method used and the concentration of precursor rhodium ions.

Introduction

In the present paper we describe some preparation methods for rhodium nanoparticles. Rhodium particles have numerous applications in important processes. They are active and selective catalysts for hydrogenation of unsaturated compounds,[1,2] Fischer−Tropsch synthesis,[3,4] hydrogenolysis reaction,[5−8] and steam reforming in hydrocarbons.[9,10] Rhodium sols were also used as catalysts in the liquid phase, however, colloidal metals can be easily recycled when deposited on a support. The specific metal surface area, which is dependent on the size of the particles, affects the activity and sometimes the selectivity of the catalysts.

In the past few years a great variety of methods have been devised for the preparation of particles in the nanosize range (1−50 nm) and described in the literature. A common feature of these methods is protection and stabilization of the primary particles from coagulation caused by the van der Waals forces. An important role is played by stabilizing agents protecting the formed nanoparticles from aggregation, making possible the preparation of particles with a diameter measuring no more than a few nanometers.[11−22] The most commonly used stabilizing agents are surfactants and polymers, with the help of which colloidal dispersions containing particles of nanometer size range are synthesized. The most widely used colloid chemical preparation method is synthesis within the droplets of microemulsions, because droplet size may be controlled within the size range of a few times 10 nanometers.[23−27]

Micelle methods for the synthesis of subcolloidal rhodium are also available in the literature. Nakao and

* Corresponding author. Tel: +36-62-544-210. Fax: +36-544-042. E-mail: i.dekany@chem.u-szeged.hu.

[†] Nanostructured Materials Research Group of the Hungarian Academy of Science.

[‡] Department of Colloid Chemistry.

[§] Department of Solid State and Radiochemistry.

(1) Boitiaux, J. P.; Cosyns, J.; Robert, E. *Appl. Catal.* **1987**, *32*, 145.
(2) Robert, F.; Oehme, G.; Grassert, I.; Sinou, D. *J. Mol. Catal. A* **2000**, *156* (1−2), 127.
(3) Quyoum, R.; Berdini, V.; Turner, M. L.; Long, H. C.; Maitlis, P. M. *J. Catal.* **1998**, *173* (2), 355.
(4) Maitlis, P. M.; Quyoum, R.; Long, H. C.; Turner, M. L. *Appl. Catal. A* **1999**, *186* (1−2), 363.
(5) Solymosi, F.; Erdõhelyi, A. *J. Mol. Catal.* **1980**, *8*, 471.
(6) Castner, D. G.; Blackadar R. L. Somorjai, G. A. *J. Catal.* **1980**, *66*, 257.
(7) Mizuno, T.; Matsumura, Y.; Nakajima, T.; Mishima, S. *Int. J. Hydrogen Energy* **2003**, *28* (12), 1393.
(8) Wang, H. Y.; Au, C. T. *Appl. Catal.s A* **1997**, *155* (2), 239.
(9) Basset, J.-M.; Ferretti, O. A.; Lucas, C.; Candy, J. P.; Didillon B.; Le Peltier, F. *J. Mol. Catal. A* **1995**, *103* (2), 125.
(10) Coq, B.; Figueras, F. *J. Mol. Catal.* **1987**, *40*, 93.
(11) Siegel, R. W. In *Physics of New Materials; Vol. 27 of Springer Series in Materials Sciences*; Fujita, F. E., Ed.; Springer-Verlag: Berlin, 1994; p 65.
(12) Fürstner, A. *Active Metals*; VCH Publishing: Weinheim, 1996.
(13) Schmid, G. *Chem. Rev.* **1992**, *92*, 1709.
(14) Esumi, K.; Shiratori, M.; Ishizuka, H.; Tano, T.; Torigoe, K.; Meguro, K. *Langmuir* **1991**, *7*, 457.
(15) Esumi, K.; Itakura, T.; Torigoe, K. *Colloids Surf. A* **1994**, *82*, 111.
(16) Esumi, K.; Suzuki, A.; Aihara, N.; Usui, K.; Toringoe, K. *Langmuir* **1998**, *14*, 3157.
(17) Fink, J.; Kiely, C. J.; Bethell, D.; Schiffrin, D. J. *Chem. Mater.* **1998**, *10*, 922.
(18) Meguro, K.; Torizuka, M.; Esumi, K. *Bull. Chem. Soc. Jpn.* **1988**, *61*, 341.
(19) Reetz, M. T.; Helbig, W. *J. Am. Chem. Soc.* **1994**, *116*, 7401.
(20) Reetz, M. T.; Quaiser, S. A. *Angew. Chem., Int. Ed. Engl.* **1995**, *34*, 2240.
(21) Toshima, N.; Takahashi, T. *Bull. Chem. Soc. Jpn.* **1992**, *65*, 400.
(22) Hoogsteen, W.; Fokkink, L. G. J. *J. Colloid Interface Sci.* **1995**, *175*, 12.
(23) Boutonnet, M.; Kizling, J.; Stenius, P. *Coll. Surf.* **1982**, *5*, 209.
(24) Berkovich, Y.; Garti, N. *Coll. Surf. A* **1997**, *128*, 91.
(25) Fan, C.; Jang, L. *Langmuir* **1997**, *13*, 3059.
(26) Puvvada, S.; Baral, S.; Chow, G. M.; Qadri, S. B.; Ratana, B. R. *J. Am. Chem. Soc.* **1994**, *116*, 2135.
(27) Tricot, Y. M.; Fendler, J. H. *J. Am. Chem. Soc.* **1984**, *106*, 7359.

10.1021/cm0310667 CCC: $27.50
Published on Web 03/17/2004

Kaeriyama synthesized rhodium nanoparticles stabilized by various surfactants by sodium borohydride reduction in aqueous medium.[28] They studied the stability of these sols and the effect of surfactants on the size of the clusters formed. Boutonett et al. prepared rhodium particles within the droplets of a microemulsion of water/penta(ethylene glycol)-dodecyl ether/hexane. Rhodium chloride dissolved in the aqueous phase could not be reduced at room temperature by hydrazine, only by hydrogen.[29] Polymer stabilization in aqueous medium, an environment-friendly method, has also been applied.[30−33] Polymer chains irreversibly adsorbed on the surface of the particles neutralize the interactions leading to aggregation. Hirai et al. generated rhodium nanosols stabilized by poly(vinyl alcohol), poly(vinylpyrrolidone), and poly(methyl vinyl ether) by alcohol reduction under reflux.[34,35] Busser et al. prepared sols by alcohol and hydrogen reduction and studied the strength of coordination between rhodium ions and various polymers.[36] They established that too strong an interaction prevents reduction of the precursor ions, whereas a weak coordination results in the formation of large particles. They found poly(vinylpyrrolidone) and poly(2-ethyloxazoline) to be optimal stabilizing agents.

Methods for the preparation of metal-containing supported catalysts are mainly impregnation techniques;[37,38] colloid methods, however, are better suited for the size-controlled synthesis of monodisperse particles. Layered silicates and layered double hydroxides are eminently suitable for the preparation of particles with a diameter of a few nanometers on the surface and within the interlamellar space of the minerals in colloid suspensions. Particle growth within the interlamellar space is sterically hindered. Metal particles are most conveniently grown within the interlamellar space of clay minerals by the exchange of cations in the exchange positions of the clay mineral for precursor transition metal cations and by subsequent reduction.[39,40]

In our earlier works the adsorption layer at the solid/liquid interface was employed as a "nanophase reactor" for the generation of nanocrystalline metal particles and for their stabilization in the presence of the clay mineral.[41−43] The procedure consists of adsorbing the precursor ions of the nanocrystalline material in the interfacial adsorption layer of solid particles (i.e., about 1-nm thick lamellae) dispersed in liquid phase, and the synthesis is carried out at the solid−liquid interface by introducing the reducing agent. The nanoparticles can be grown attached to the surface, in well-controllable number and size, between the silicate layers. In view of the powerful stabilizing effect of polymers, we set out to test the joint stabilizing effect of the polymer/clay mineral complex in the preparation of Pd^0 nanoparticles. We showed that monodisperse particles can be obtained, the size of which depends on polymer and precursor ion concentrations.[44,45]

We also prepared nanosized palladium particles in the interlamellar space of kaolinite. Kaolinite, a nonswelling mineral in water, was disaggregated by DMSO.[46] The large surface area necessary for nanoparticle growth may be created by breaking up the hydrogen bonds tightly interlinking the kaolinite lamellae, i.e., by disaggregating the sample. Gábor at al. obtained the intercalation complex of kaolinite with hydrazine and potassium acetate.[47] Komori et al. cleaved interlamellar hydrogen bonds in kaolinite by *N*-methylformamide (NMF).[48,49] In the present work, homogeneous and heterogeneous nucleation procedures for the preparation of rhodium nanoparticles are described (see Figure 1). These methods share the common characteristics of using an aqueous medium and tailoring particle growth and preventing aggregation by the addition of neutral and ionic polymers. In the case of homogeneous nucleation, it is important to take into account the concentration of precursor ions and their interaction with the stabilizing polymer, especially if the latter is an ionic polymer, because the reduction rate of metal ions in solutions of polymers and, consequently, particle size are affected by electolytic interactions. In the case of heterogeneous nucleation, the interactions to be characterized are those between polymer and support, between polymer and precursor, and between polymer, support and precursor. Adsorption of precursor ions on the silicate lamellae of the support (kaolinite, montmorillonite) has an influence on particle size; however, the effect of the polymer adsorbed on the surface of the support also has to be considered, as these may be adsorbed not only in the interlamellar space (montmorillonite) but also on the edges, in accordance with the electrostatic interactions operating between polymer and silicate. Thus, anionic, cationic, and neutral polymers may play different roles on layered silicates with negative surface charge.

The effect of the electric charge, the molecular mass, and the concentration of polymers on the size of the particles and their adsorption on the surface of montmorillonite and kaolinite supports was studied. Particle size of Rh^0 nanoparticles was determined by transmission electron microscopy and the metal/polymer/clay mineral composites were characterized by X-ray diffraction, XPS, and SAXS experiments.

(28) Nakao, Y.; Kaeriyama, K. *J. Colloid Interface Sci.* **1986**, *110*, 82.
(29) Boutonnet, M.; Kizling, J.; Stenius, P. *Colloids Surf.* **1982**, *5*, 209.
(30) Teranishi, T.; Miyake, M. *Chem. Mater.* **1998**, *10*, 594.
(31) Liu, H.; Mao, G.; Meng, S. *J. Mol. Catal.* **1992**, *74*, 275.
(32) Yu, W.; Lin, H. *Chem. Mater.* **1998**, *10*, 1205.
(33) Chen, C.-W.; Akashi, M. *Langmuir* **1997**, *13*, 6465.
(34) Hirai, H.; Nakao, Y.; Toshima, N. *J. Macromol. Sci. Chem.* **1978**, *A12* (8), 1117.
(35) Hirai, H. *J. Macromol. Sci. Chem.* **1979**, *A13* (5), 633.
(36) Busser, G. W.; van Ommen, J. G.; Lercher, J. A. *J. Phys. Chem. B* **1999**, *103* (10), 1651.
(37) Campelo, J. M.; Garcia, A.; Luna, D.; Marinas, J. M. *Colloids Surf.* **1982**, *5*, 227.
(38) Solymosi, F.; Tombácz, I.; Kocsis, M. *J. Catal.* **1982**, *75*, 78.
(39) Aihara, N.; Torigoe, K.; Esumi, K. *Langmuir* **1998**, *14*, 4945.
(40) Malla, P. B.; Ravindranathan, P.; Komarneni, S.; Roy, R. *Nature* **1991**, *351*, 555.
(41) Dékány, I.; Turi, L.; Szûcs, A.; Király, Z. *Colloids Surf. A* **1998**, *141*, 405.
(42) Szûcs, A.; Király, Z.; Berger, F.; Dékány, I. *Colloids Surf. A* **1998**, *139*, 109.
(43) Dékány, I.; Turi, L.; Király, Z. *Appl. Clay Sci.* **1999**, *15*, 221.
(44) Papp, S.; Szûcs, A.; Dékány, I. *Appl. Clay Sci.* **2001**, *19*, 155.
(45) Papp, S.; Szûcs, A.; Dékány, I. *Solid State Ionics* **2001**, *141−142*, 169.
(46) Papp, S.; Dékány, I. *Prog. Colloid Polym. Sci.* **2001**, *117*, 94.
(47) Gábor, M.; Tóth, M.; Kristóf, J.; Komáromi-Hiller, G. *Clays Clay Miner.* **1995**, *43* (2), 223.
(48) Komori, Y.; Sugahara, Y.; Kuroda, K. *Chem. Mater.* **1999**, *11*, 3.
(49) Komori, Y.; Sugahara, Y.; Kuroda, K. *Appl. Clay Sci.* **1999**, *15*, 241.

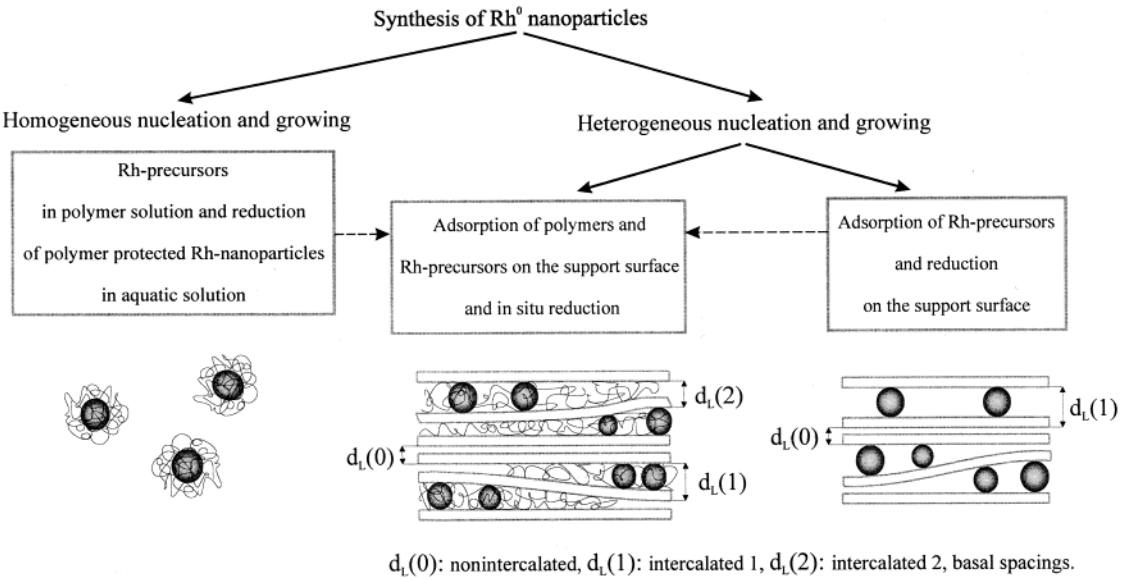

Figure 1. Applied synthesis methods for Rh^0 nanoparticle preparation.

Table 1a. Particle Size of Neutral-Polymer-Protected Rh^0-Nanosols and Basal Spacing of Rh^0/Polymer/Clay Samples

	PVP (M_w = 40 000)									
Rh/monomer molar ratio	1:1						1:5		1:20	
	Rh^0-nanosols									
c_{RhCl3} (mmol/l)[a]	0.1		0.2		0.4		0.2		0.2	
d_{ave} (nm)[b]			1.64 ± 0.48		2.69 ± 0.99		1.97 ± 0.52		1.6 ± 0.76	
	Support: Montmorillonite									
Rh content (wt %)	0.5		1.0		2.0		1.0		1.0	
basal spacing/rel intensity[c]	d_L (nm)	I_{rel} (%)	d_L (nm)	I_{rel} (%)	d_L (nm)	I_{rel} (%)	d_L (nm)	I_{rel} (%)	d_L (nm)	I_{rel} (%)
intercalated 1	3.51	18.3	3.59	31.4	3.62	34.7	3.68	19	3.81	48.6
intercalated 2							2.5	24.5	2.5	51.4
nonintercalated	1.49	81.7	1.46	68.6	1.37	65.3	1.5	56.6		
d_{ave} (nm) TEM	1.79 ± 0.5		2.48 ± 0.72		3.06 ± 0.89		2.74 ± 0.56		1.79 ± 0.41	
	Support: Kaolinite									
Rh content (wt %)	0.5		1.0		2.0		1.0		1.0	
basal spacing/rel intensity	d_L (nm)	I_{rel} (%)	d_L (nm)	I_{rel} (%)	d_L (nm)	I_{rel} (%)	d_L (nm)	I_{rel} (%)	d_L (nm)	I_{rel} (%)
intercalated 1	3.92	28.5	3.73	25.8	3.78	33	3.65	27.5	4.03	37.6
intercalated 2	2.79	21.4	2.77	22.2			2.72	23.1	2.74	21.6
nonintercalated	0.72	49.8	0.73	52	0.73	67	0.73	49.4	0.72	40.8
d_{ave} (nm) TEM	1.37 ± 0.36		1.45 ± 0.41		1.15 ± 0.32		1.42 ± 0.38		1.11 ± 0.31	

[a] c_{RhCl3}: precursor concentration in polymer solution. [b] d_{ave}: average diameter of Rh^0 nanoparticles determined by TEM experiments. [c] $I_{rel} = I_{int}/(I_{int} + I_{nonin}) \times 100$.

Experimental Section

Materials. Fine fraction of sodium montmorillonite, $d < 2$ μm (Süd-Chemie AG, Moosburg, Germany), and kaolinite, $d = 10-20$ μm (Zettlitz, Germany), were used as support layered silicates for the preparation of nanoparticles. Specific surface area was determined by N_2 adsorption measurements, and the results were $a^S_{BET} = 87.7$ m^2/g and $a^S_{BET} = 14$ m^2/g for Na-montmorillonite and kaolinite, respectively. Air-dried samples were characterized by X-ray diffraction. The basal spacings were $d_L = 1.44$ nm for the Na-montmorillonite and $d_L = 0.72$ nm for the kaolinite sample. Dimethyl sulfoxide (DMSO, analytical purity, Reanal, Hungary) was used for delamination of the kaolinite particles. The metal precursor rhodium(III) chloride hydrate (purity 98%) and the reducing agent sodium borohydride (purity 99%) were obtained from Aldrich. Three different polymers were used to stabilize the Rh^0 nanoparticles: poly(*N*-vinyl-2-pyrrolidone) (PVP, K-30, average molecular weight 4×10^4, Fluka), 20 wt % aqueous solution of poly(diallyldimethylammonium chloride) (PDDA, three average molecular weights: 10^5 to 2×10^5(low), 2×10^5 to 3.5×10^5 (medium), and 4×10^5 to 5×10^5 (high), Aldrich) and poly(sodium 4-styrenesulfonate) (PSSN, two average molecular weights: 7×10^4 and 10^6, Aldrich).

Preparation of Rh^0 Nanoparticles. *Polymer-Stabilized Rh^0 Nanosols.* Rhodium nanosols were prepared at room temperature from an aqueous solution of $RhCl_3$ with $NaBH_4$ as reducing agent. Freshly prepared $NaBH_4$ solution was added to rhodium at a molar ratio of 1:12. The nanoparticles formed by homogeneous nucleation were stabilized by the addition of polymers. PVP was added to the rhodium solution at Rh/PVP monomer ratios of 1:1, 1:5, and 1:20, at three different rhodium concentrations (0.1, 0.2, and 0.4 mM). Cationic PDDACl of three and PSSN of two different molecular masses were used only at one Rh/PDDACl/PSSN monomer ratio, 1:1 (see Table 1a and b). Aqueous rhodium chloride solution (2 mM) was added to the aqueous polymer solution (0.01 g/100 mL); the mixture was stirred for 2 h, and the precursor ions were reduced by freshly prepared 13 mM sodium borohydride solution. Reduction led to the formation of brown-black Rh^0 nanosols.

Polymer-Stabilized Rh^0 Nanoparticles on Montmorillonite. Rhodium nanoparticles were prepared on the lamellae of montmorillonite by heterogeneous nucleation, at the R/monomer ratios specified above (see Table 1a and b). Na-montmorillonite was suspended in aqueous polymer solution and stirred at room temperature for 24 h. Rhodium chloride solution was added to the polymer/montmorillonite composite in amounts corresponding to 0.5, 1.0, and 2.0 wt % with respect to the support; the mixture was stirred for 2 h and a 12-fold excess of 13 mM $NaBH_4$ was then added. The concentration

Table 1b. Particle Size of Ionic-Polymer-Protected Rh^0-Nanosols and Basal Spacing of Rh^0/Polymer/Clay Samples

	PDDA (cationic)						PSSN (anionic)			
molecular weight	low		med		high		70 000		1 000 000	
Rh/monomer molar ratio					1:1					
					Rh^0-nanosols					
c_{RhCl3} (mmol/l)[a]	0.2		0.2		0.2		0.2		0.2	
d_{ave} (nm)[b]	1.94 ± 0.87		1.52 ± 0.47		1.38 ± 0.54		2.87 ± 0.91		2.86 ± 0.89	
					Support: Montmorillonite					
Rh content (wt %)					1.0					
basal spacing/rel intensity[c]	d_L (nm)	I_{rel} (%)	d_L (nm)	I_{rel} (%)	d_L (nm)	I_{rel} (%)	d_L (nm)	I_{rel} (%)	d_L (nm)	I_{rel} (%)
intercalated 1	3.62	26.2	3.71	36.9	3.91	47.2	3.45	17.9	3.56	19.7
nonintercalated	1.49	73.8	1.48	63.1	1.48	52.8	1.48	81.2	1.48	80.3
d_{ave} (nm) TEM	1.87 ± 0.52		1.24 ± 0.31		1.67 ± 0.45		2.21 ± 0.57		2.42 ± 0.49	
					Support: Kaolinite					
Rh content (wt %)					1.0					
basal spacing/rel intensity	d_L (nm)	I_{rel} (%)	d_L (nm)	I_{rel} (%)	d_L (nm)	I_{rel} (%)	d_L (nm)	I_{rel} (%)	d_L (nm)	I_{rel} (%)
intercalated 1	3.26	21.1	3.66	32.4	3.69	26.7	3.97	24.7	3.78	29.1
intercalated 2	2.63	24.8	2.82	26.5	2.72	22.5			2.82	23.4
nonintercalated	0.73	54.1	0.73	41.1	0.73	50.8	0.73	75.3	0.73	47.5
d_{ave} (nm) TEM	1.2 ± 0.23		1.29 ± 0.33		1.88 ± 0.46		1.17 ± 0.36		1.37 ± 0.51	

[a] c_{RhCl3}: precursor concentration in polymer solution. [b] d_{ave}: average diameter of Rh^0 nanoparticles determined by TEM experiments. [c] $I_{rel} = I_{int}/(I_{int} + I_{nonint}) \times 100$.

of montmorillonite in the suspension was 1 g/100 mL. The compositions of the Rh/polymer/montmorillonite composites are listed in Table 1a and b.

Polymer-Stabilized Rh^0 Nanoparticles on Kaolinite. The kaolinite was expanded by the intercalation of DMSO at T = 65 °C. The excess of DMSO was removed from the sample by several washings with methanol within 5 days. Rh/kaolinite composites were prepared directly by reduction of Rh^{3+} ions previously adsorbed in the MeOH/DMSO/kaolinite system. Intercalation complexes of polymer/kaolinite were prepared in aquatic solution at various concentrations of PVP, PDDA, and PSSN by polymer adsorption at room temperature in a 24-h reaction at constant stirring. Rh/polymer/kaolinite composites were prepared by applying different polymers in 0.005−0.2 g/100 mL concentrations (see Table 1a and b) adsorbed on MeOH/DMSO/kaolinite at 1.0 g/100 mL concentration from an aquatic dispersion which was followed by adsorption and reduction of Rh^{3+} ions. Kaolinite samples containing different amounts of rhodium (0.5−2.0 wt %) were obtained by $NaBH_4$ reduction at 1:12 Rh^{3+}/$NaBH_4$ ratio.

Analytical Methods. *Absorption Spectrophotometry.* Growth of the rhodium nanoparticles by Na-borohydride reduction in PVP solution was followed by absorption spectrophotometry. UV−Vis spectroscopy was carried out in a dual-beam Uvikon 930 spectrophotometer. Rh^0 sol was studied in 10-mm quartz cuvettes. The system to be studied was placed in one light path, the reference system was placed in the other, and the difference spectrum was recorded in the range of 190−300 nm.

XRD Experiments. X-ray diffraction measurements were taken on a Philips PW 1820 diffractometer, with Cu Kα radiation (λ = 0.154 nm) being used at 40 kV and 35 mA in 2θ range $1° \le 2\theta \le 50°$. The basal distances d_L were calculated from the first (001) Bragg reflections by using the PW 1877 automated powder diffraction software.

Transmission Electron Microscopy (TEM). Images were made in a Philips CM-10 transmission electron microscope with an accelerating voltage of 100 kV. Aliquots of the ethanol suspensions of the samples were dropped on copper grids (diameter 2 mm) covered with Formwar foil, which were then left to stand for 3−40 s and transferred into the microscope. Particle size distribution was determined by using the UTH-SCSA Image Tool program.

Small-Angle X-ray Scattering (SAXS). SAXS was measured by the same radiation as in the case of XRD. The primary beam was directed through a Ni-filter into a compact Kratky camera, type KCEC/3, in which the width of the beam was 20 mm and its thickness was 80 μm. The measurements were done in a vacuum atmosphere. The intensity of the scattered radiation was measured by a proportional detector (slit width 100 μm) controlled by a PW 1710 microprocessor, and SDC (Scattering Data Controlling) software, in an angle range of 2θ = 0.05−7°. Absorption intensities (A_s, A_b) were determined by the so-called moving slit method.[51] The I(h) scattering function measured in the Kratky camera had to be normalized and the background scattering had to be taken into consideration to determine structural parameters.

X-ray Photoelectron Spectroscopy (XPS). XPS measurements were performed in the ultrahigh vacuum chamber ($p = 2 \times 10^{-9}$ mbar) of a Kratos XSAM 800 instrument equipped with a hemispherical analyzer. Al Kα radiation ($h\nu$ = 1486.6 eV) was used as the excitation source. The gun was operated at 15 kV and 15 mA. The pass energy of the electron analyzer was set to 40 eV, and the step width between the channels was 50 meV. Usually 10 scans were added to give a single spectrum. All binding energies were referenced to the C (1s) line of the adventitious carbon assumed to have a constant binding energy of 285.1 eV. Data acquisition and evaluation were performed with the VISION 1.3.3 software provided by Kratos Ltd.

Results and Discussions

Because the reduction of rhodium ions by sodium borohydride has been formulated in several different ways in the literature, the amount of reducing agent necessary for complete conversion was also determined. To a 0.2 mM rhodium chloride solution containing 0.01 g/100 mL PVP, a 13 mM (0.05 g/100 mL) solution of the reducing agent was added in aliquots of 20 μL with constant stirring. The process of reduction at different $NaBH_4$ concentrations—after 1 min reaction time—can be followed on the UV−Vis spectra shown in Figure 2. The peaks characteristic of the chloro complexes of rhodium (225 and 198 nm) gradually disappear, accompanied by a gradual rise of the descending branch of the spectrum (in the range of 260−300 nm), due to particle formation. At high excesses of the reducing agent the new peak characteristic of Rh^0 nanoparticles appears at 194 nm. By the evidence of this experiment, Na-borohydride has to be added in a 12-fold excess over rhodium ions in order for the reaction to proceed to completion.

(50) Papp, S.; Dékány, I. *Colloid Polym. Sci.* **2003**, *281*, 727.
(51) Stabinger, H.; Kratky, O. *Makromol. Chem. Phys.* **1978**, *179* (6), 1655.

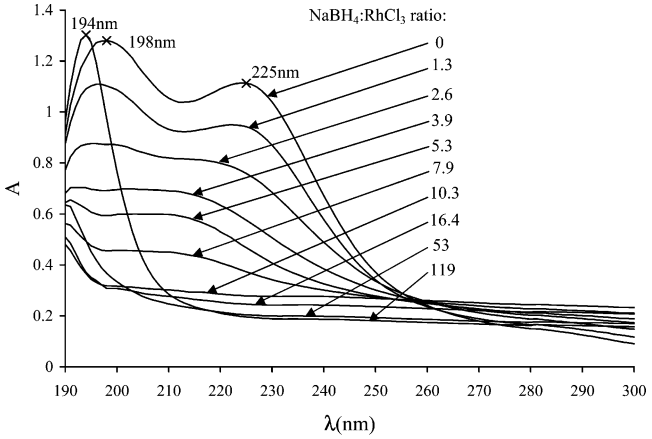

Figure 2. Determination of necessary amount of $NaBH_4$ for total reduction of Rh^{3+} ion by adsorption spectrophotometry. The curve shows the 1:10 $Rh^{3+}/NaBH_4$ ratio is necessary for the total reduction.

The sols prepared in these experiments are characterized in Table 1a and b. A stable, brown-black sol was obtained in each case, except for the system containing 0.1 mM rhodium stabilized by PVP. Reductions were rapidly completed (1−4 s). According to the electron microscopic size analysis, particles measuring 1−3 nm were formed (Figure 3a). As the amount of PVP added is increased, particle size does not change considerably. In our earlier experience the rate of reduction is decreased when the amount of polymer added exceeds that necessary for full stabilization, and this decrease in the rate of reduction may even result in an increase in particle size.[50]

When rhodium concentration is increased from 0.2 to 0.4 mM at a Rh/monomer ratio of 1:1, stabilized primary particles probably aggregate to form secondary particles, leading to an increase in average particle size (from 1.64 to 2.69 nm).

In sols stabilized by PDDA, as molecular mass is increased, smaller particles are formed. According to Hoogsteen, in the case of a strong precursor−polymer interaction (Pd particles stabilized by PVP) particle size is determined by monomer number rather than molecular mass.[22] In Busser's opinion, size is decreased when molecular mass is smaller, due to the possibility of multiple adsorption.[36] We have found no data in the literature concerning particle size in metal sols stabilized by PDDA or other cationic polymers. There are no significant differences between the molecular masses of the PDDA fractions studied by us; the positively charged precursor ions may not be strongly bound to the positively charged functional group. It is probably for steric reasons that primary particles are unable to aggregate, which keeps particle size relatively low. At a rhodium concentration of 0.2 mM and a Rh/:monomer ratio of 1:1, particle size obtained using the PDDA fraction with the lowest molecular mass ($M_w = 10^5$ to 2×10^5) is larger than that obtained in the presence of PVP. This may be caused by the repulsive $Rh^{3+}-PDDA^+$ interaction. The largest particles were obtained in systems stabilized with PSSN. The explanation based on Busser's work for this phenomenon is that the strongest interaction is established between the negatively charged PSSN and Rh(III) ions, decreasing the rate of reduction and resulting in a larger particle size.[36] In these cases, increasing the molecular mass of the polymer did not result in a decrease in particle size (2.86−2.87 nm); however, particles assemble into relatively large strings (Figure 3b).

Nanoparticles were also prepared on montmorillonite, at Rh/monomer ratios corresponding to those used in

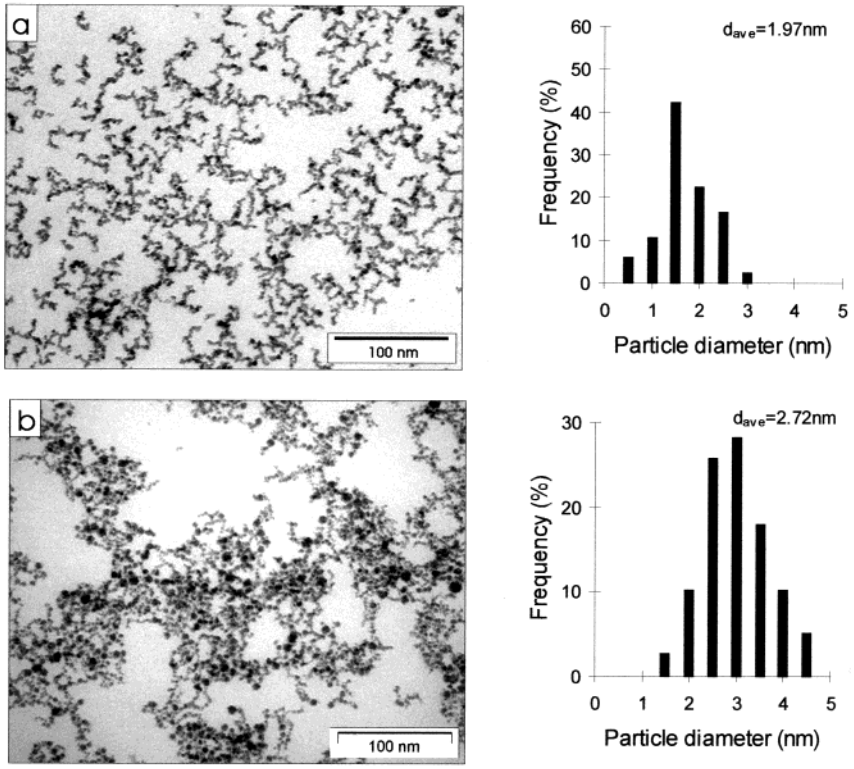

Figure 3. TEM image and particle size distribution of PVP-stabilized Rh nanosol (Rh/PVP molar ratio = 1:5) (a); PSSN70-stabilized Rh nanosol (b).

Table 2a. Basal Spacing of Neutral Polymer/Clay Samples

	PVP (M_w = 40 000)									
Polymer content (wt %)	0.54		1.08		2.16		5.39		21.5	
Support: Montmorillonite										
basal spacing/rel intensity[a]	d_L (nm)	I_{rel} (%)	d_L (nm)	I_{rel} (%)	d_L (nm)	I_{rel} (%)	d_L (nm)	I_{rel} (%)	d_L (nm)	I_{rel} (%)
intercalated 1									3.91	16.7
intercalated 2									2.58	32.6
nonintercalated	1.53	100	1.53	100	1.55	100	1.56	100	1.58	50.7
Support: Kaolinite										
basal spacing/rel intensity	d_L (nm)	I_{rel} (%)	d_L (nm)	I_{rel} (%)	d_L (nm)	I_{rel} (%)	d_L (nm)	I_{rel} (%)	d_L (nm)	I_{rel} (%)
intercalated 1	3.78	39.1	3.78	33.1	3.44	33.4	3.68	29.6	3.73	40.4
nonintercalated	0.72	60.9	0.72	66.9	0.73	66.6	0.73	70.4	0.73	49.6

[a] $I_{rel} = I_{int}/(I_{int} + I_{nonint}) \times 100$.

Table 2b. Basal Spacing of Ionic Polymer/clay Samples

	PDDA (cationic)						PSSN (anionic)			
molecular weight	low		med		high		70 000		1 000 000	
polymer content (wt %)	0.54		1.08		2.16		5.39		21.5	
Support: Montmorillonite										
basal spacing/rel intensity[a]	d_L (nm)	I_{rel} (%)	d_L (nm)	I_{rel} (%)	d_L (nm)	I_{rel} (%)	d_L (nm)	I_{rel} (%)	d_L (nm)	I_{rel} (%)
intercalated 1					4.31	9.6	3.64	8.4	3.98	6.8
nonintercalated	1.53	100	1.55	100	1.54	90.4	1.53	91.6	1.54	93.2
Support: Kaolinite										
basal spacing/rel intensity	d_L (nm)	I_{rel} (%)	d_L (nm)	I_{rel} (%)	d_L (nm)	I_{rel} (%)	d_L (nm)	I_{rel} (%)	d_L (nm)	I_{rel} (%)
intercalated 1					5.95	21	3.64	26.2	3.78	29.6
nonintercalated	0.73	100	0.73	100	0.73	79	0.73	73.8	0.72	70.4

[a] $I_{rel} = I_{int}/(I_{int} + I_{nonint}) \times 100$.

the preparation of sols. By the evidence of XRD pictures, basal spacing in air-dried montmorillonite is $d_L = 1.48$ nm, due to the presence of adsorption water between the lamellae. Incorporation between the lamellae of montmorillonite was observed only at the highest PVP content applied (21.5 wt %) (Table 2a). However, the structure of montmorillonite is significantly altered by the formation of rhodium particles (Figure 4a and b). The intensity of the original reflection of montmorillonite (1.48 nm) decreases, that of the new reflection (at $d_L = 3.8$ nm) increases, and the location of the latter is slightly shifted (d_L = 3.4−4.0 nm). With PVP as stabilizing agent, another new peak appears at about $d_L = 2.5$ nm as the monomer/Rh ratio is increased; at a ratio of 20:1 the original reflection of montmorillonite disappears and the structure is completely altered (Figure 4b). The second reflection appearing at large angles is indicative of a fraction of smaller particles, also verified by a decrease in average size (see schematic picture on Figure 1). At high PVP content (21.5 wt %), as well as in the presence of the anionic PSSN, part of the particles were not adsorbed on the surface of the support. Part of the large amount of PVP added could not bind to the support or intercalate, thus this excess polymer stabilized the newly formed particles in the bulk phase. In the case of PSSN, Rh^0 particles are practically not bound to the surface of the montmorillonite due to repulsion by negative charges. No intercalation is observed on the X-ray diffractograms of these samples and the size of rhodium particles is not affected by the presence of the support. In the case of PDDA, increase in molecular mass, i.e., incorporation of monomers in larger units, is preferential (Figure 4a). Longer chains opened up longer stretches of the lamellae, drawing more particles into the interlamellar space. Systematic variation of molecular mass did not bring about unequivocal changes in particle size (Table 1b, Figure 5a). When metal content is increased (0.5−2 wt %) at a Rh/PVP monomer ratio of 1:1, the intensity of the original reflection decreases and the peak becomes broader, indicating a decrease in the orderedness of the structure. As metal content was increased, average particle size increased by 0.7−1.3 nm, whereas basal spacing increased only by 0.1−0.2 nm (3.5→3.6 nm) (Figure 5b, Table 1a). As we have formerly described, in PVP/montmorillonite/rhodium composites the increase in particle size with increasing metal content may also be a consequence of polymer−support interactions.[50] A fraction of the polymer chains is adsorbed on the surface before the addition of Rh^{3+} ions, therefore the polymer molecules remaining in the bulk phase can stabilize the nascent particles—which will attach to the surface of the support as soon as they are formed—only at a low Rh/monomer ratio. This is why a reaction medium containing montmorillonite and a relatively low amount of strongly adsorbing polymer (PVP, PDDA) will yield particles of higher average size than would homogeneous nucleation. In this case heterogeneous nucleation is no longer the case.

Polymer-free samples with metal contents of 0.5, 1.0, and 2.0 wt % were also prepared. The intensity of the montmorillonite reflection (001) is not seen to decrease on the X-ray diffractograms, indicating that the majority of the particles grew on the external surfaces, leaving the original basal spacing of the support unchanged (Table 3). Partial incorporation of particles is revealed

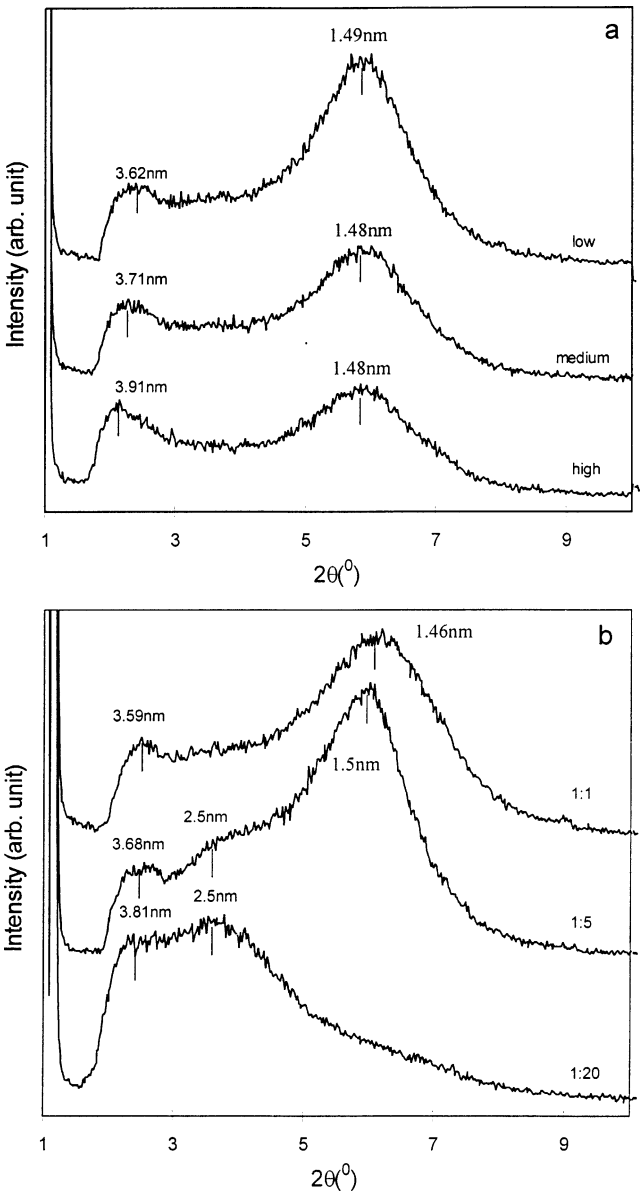

Figure 4. XRD patterns of the PDDACl-protected Rh^0-montmorillonite at different molecular weights (a); PVP-protected Rh^0-montmorillonite at different polymer contents (b) showing Rh^0 nanoparticles intercalated in the interlamellar space.

by the shift in the position of the emerging shoulder (d_L = 3.8 nm→5.0 nm). It can be established that montmorillonite structure is altered to a much higher extent when polymers (PVP or PDDA) are used for the synthesis of Rh^0 (30−50%) than when only the polymer or only rhodium is present (10−20%). Particle size is slightly decreased with increasing metal content (Table 3). The rate of nucleation was increased by increasing precursor concentration, therefore particle size decreased on the support with large specific surface area. In this case particles are formed on the surface of lamellae situated a fixed distance from each other, restricting particle growth, rather than in the bulk phase protected by the polymer, as in the case of synthesis in the presence of polymers.

Rhodium nanoparticles were also grown on kaolinite, using similar techniques. To create the space necessary for the synthesis of nanoparticles, the hydrogen bonds tightly interlinking the kaolinite lamellae must be broken up. Disaggregation was nearly 100% complete after the formation of the DMSO/kaolinite intercalation complex. Changes in the basal spacing of kaolinite were studied in the range of l° < 2θ < 14°. X-ray diffraction measurements revealed that basal spacing increased from 0.72 to 1.12 nm within 24 h at 65 °C (Figure 6a). Interlamellar distance was unchanged after removal of DMSO molecules hindering particle synthesis from the interlamellar space. The MeOH/kaolinite complex obtained in this way was used as an intermediate in further preparations. The 1.2-nm reflection of delaminated kaolinite disappears in aqueous medium and the lamellae are partially rearranged (84%) to their original position, an interlamellar distance of 0.72 nm (Figure 6a). We studied polymer incorporation between the disaggregated kaolinite lamellae (Table 2a and b). By the evidence of the X-ray diffractograms, the macromolecules (with the exception of PDDA) were also incorporated among the kaolinite lamellae. Considering the specific surface area and the ion exchange capacity of kaolinite are low (14 m^2/g and 6−8 meqv/g, respectively), this may mean the incorporation of only a small percentage of the molecular chains. Polymers are adsorbed not only on the external surfaces of the support but also on the internal surfaces lining the interlamellar space, pushing part of the lamellae apart to a distance of ∼3.7 nm (Table 1a and b). When rhodium particles protected by polymers added in the above-specified quality and quantity are grown, a new peak appears at $d_L \approx 2.7$ nm in all cases. When the amount of PVP added is increased, the structure is dilated to an increasing extent, the relative intensity of the peak appearing at smaller angles increases, and the peak is shifted to 4.02 nm (Figure 6b). At a Rh/monomer ratio of 1:20, as much as 60% of the structure is opened up. In the case of the cationic PDDA, molecular mass was varied. The effect of increasing chain length on structure was similar to that of increasing PVP concentration. When low-molecular-weight PDDACl is used, of the two new peaks (at 3.26 and 2.63 nm) the intensity of the one at 2.63 nm is higher, indicating that shorter polymer chains are incorporated between the lamellae in smaller units (Figure 6c). As chain length is increased, the intensity of the peak at smaller angles increases, because larger polymer coils need more space. Maximal incorporation (60%) is observed at medium molecular masses. PSSN, an anionic polymer is not capable of binding to the negatively charged surface of kaolinite. Diffractograms of Rh^0 samples synthesized in the presence of PSSN show little intercalation (25%); even in this case, however, relatively longer chains have opened up a sizable fraction of the lamellae (50%) (see Table 1b). When metal content is increased (0.5−2.0 wt %) at a Rh/PVP monomer ratio of 1:1, out of the two basal spacing values indicating two different initial particle sizes it is the intensity of the peak appearing at larger angles that is increased. At 2.0 wt % metal content the peaks are no more separable. TEM pictures show that average particle size was somewhat reduced by higher precursor and polymer concentrations (d_{ave} = 1.4→1.1 nm), whereas increasing molecular mass resulted in the formation of larger particles (d_{ave} = 1.2→1.9 nm) (Figure 7a). Particles in kaolinite/rhodium/PVP−PSSN composites are smaller than those on montmorillonite. Because

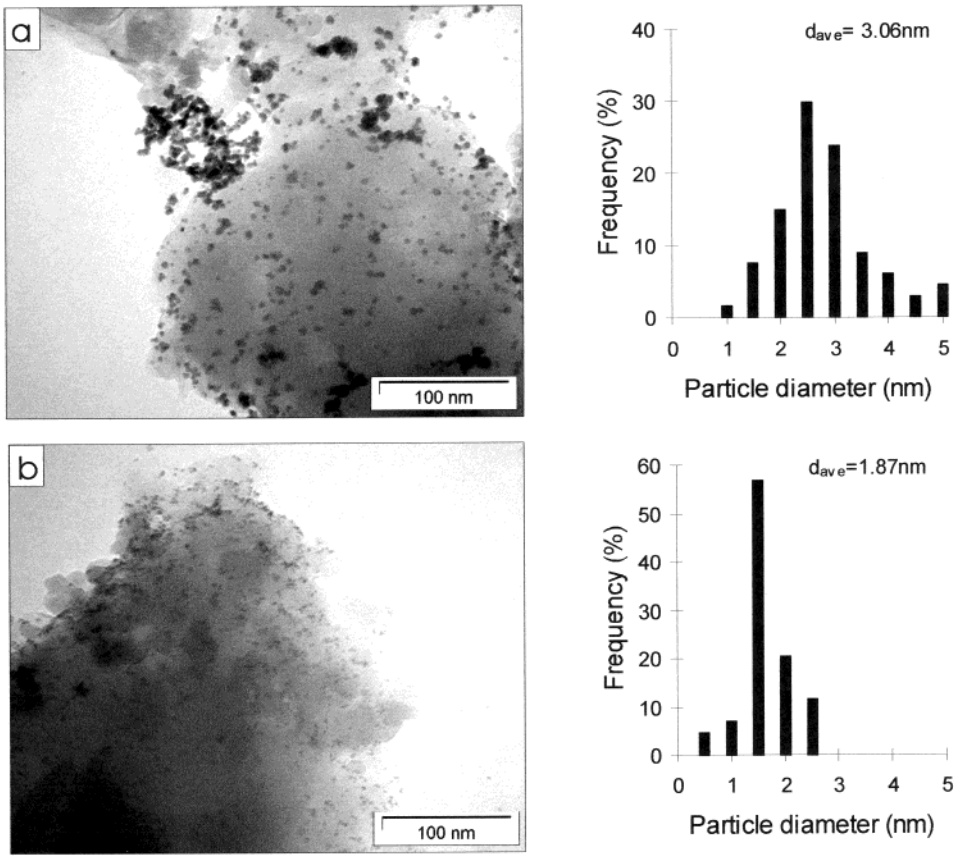

Figure 5. TEM image and particle size distribution of low-molecular-weight PDDACl-protected Rh^0-montmorillonite (1 wt % Rh) (a); PVP-protected Rh^0-montmorillonite (2 wt % Rh) (b).

Table 3. Particle Size and Basal Spacing of Rh^0/clay Samples

Rh content (wt %)	0		0.5		1.0		2.0	
			Support: Montmorillonite					
basal spacing/rel intensity[a]	d_L (nm)	I_{rel} (%)	d_L (nm)	I_{rel} (%)	d_L (nm)	I_{rel} (%)	d_L (nm)	I_{rel} (%)
intercalated 1			4.08	19	4.8	18.1	4.96	22.6
nonintercalated	1.48	100	1.51	81	1.57	81.9	1.62	77.4
d_{ave} (nm) TEM[b]			2.23 ± 0.49		1.7 ± 0.46		1.62 ± 0.67	
			Support: Kaolinite					
basal spacing/rel intensity	d_L (nm)	I_{rel} (%)	d_L (nm)	I_{rel} (%)	d_L (nm)	I_{rel} (%)	d_L (nm)	I_{rel} (%)
intercalated 1			3.62	43.1	3.69	45.6	3.92	32.2
nonintercalated	0.73	100	0.72	56.9	0.72	54.4	0.73	67.8
d_{ave} (nm) TEM			1.41 ± 0.31		1.34 ± 0.43		1.1 ± 0.32	

[a] $I_{rel} = I_{int}/(I_{int} + I_{nonint}) \times 100$. [b] d_{ave}: average diameter of Rh^0 nanoparticles determined by TEM experiments.

of its lower surface charge density (especially on the edges), kaolinite is neutral and can adsorb fewer negative polymer chains, which means that more remains in the bulk phase to stabilize the particles.

Kaolinite samples with 0.5−2.0 wt % rhodium content were also prepared without polymer stabilization (Figure 7b). In the samples containing 0.5 and 1.0 wt % Rh, over 40% of the structure of kaolinite was transformed due to intercalation, a result never achieved with either polymer (Table 3). In contrast, at small angles a single peak characteristic of one value of basal spacing is observed, similarly to composites containing only polymer (Figure 6d). Average particle sizes were nearly identical to that of nanoparticles synthesized at a PVP monomer/rhodium ratio of 1:1. This amount of PVP had no effect on synthesis. Is it possible that particles are formed independently of previously incorporated polymer molecules on different interlamellar surfaces. The average particle sizes are smaller on kaolinite than on montmorillonite, because adhesion forces operating between kaolinite lamellae are stronger.

Changes in the structural properties of clay minerals and the presence of nanoparticles or polymer chains on the support may also be detected by SAXS experiments (see Appendix). Measurements were started with supports samples without nanoparticles and polymers determined. SAXS parameters calculated from the log $I = f(\log h)$ representations and $I \times h^3 = f(h^3)$ (so-called Porod representations) are given in Table 4. The $\log(I) - \log(h)$ scattering functions of montmorillonite and kaolinite demonstrate well the difference between the two types of clay minerals. The scattering intensity (I) and the slope of the curve are smaller for montmorillonite than for kaolinite. The surface fractal dimensions

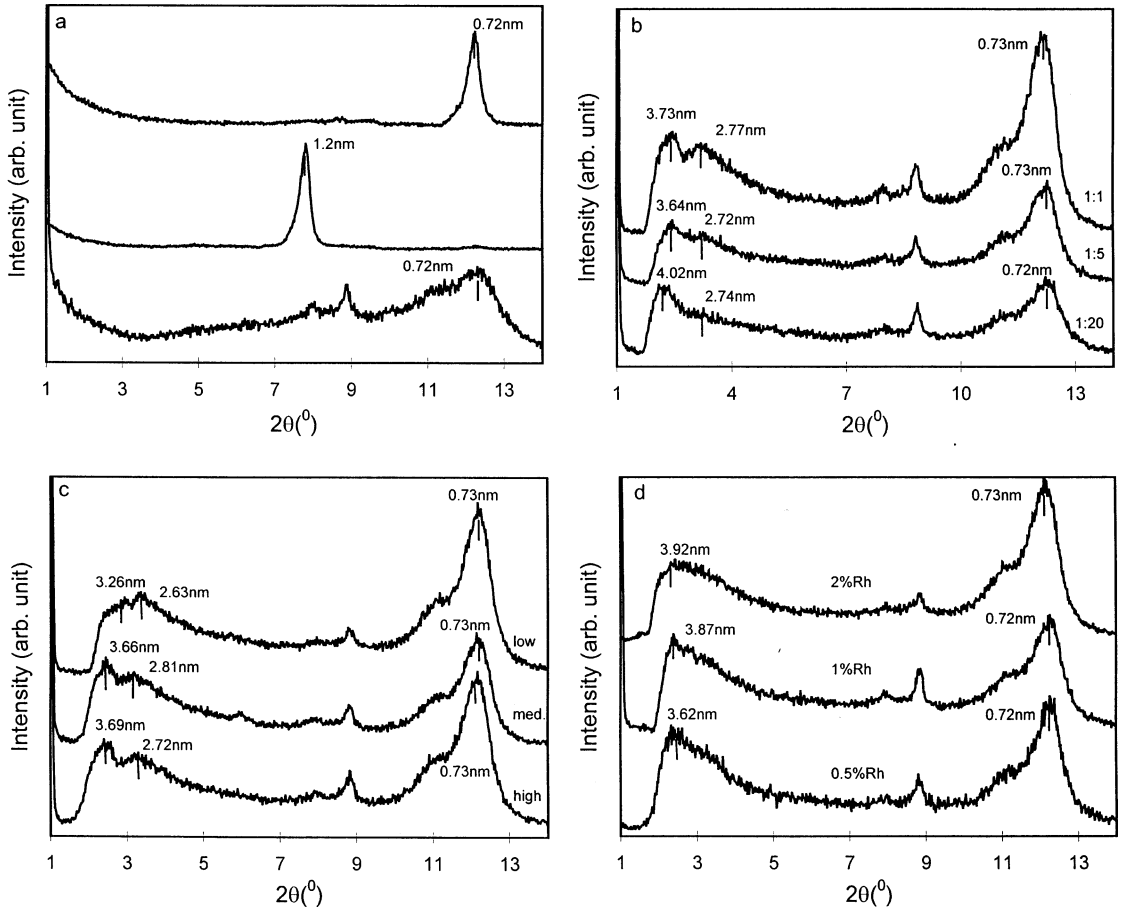

Figure 6. XRD patterns of the kaolinite, DMSO/kaolinite, and rehydrated kaolinite (a); PVP-protected Rh^0-kaolinite at different polymer contents (b); PDDACl-protected Rh^0-kaolinite at different molecular weights (c); Rh^0-kaolinite at different Rh^0 contents (d) showing Rh^0 nanoparticles intercalated in the interlamellar space.

(D_s) calculated from the slope of the curve are the following: D_s(kaolinite) = 2.417, D_s(montmorillonite) = 2.909 (see appendix after eq 7). In the case of a smooth surface, the value of the surface fractal dimension is D_s = 2.0. Thus, in our case the surface of kaolinite is not smooth, but will be uneven, and the surface of montmorillonite is much rougher. These values are further enhanced by introduction of PVP and Rh^0 nanoparticles (Table 4). The intensity of X-ray scattering is enhanced by the higher electron density of metal nanoparticles located on the surface, therefore intensity is seen to increase with increasing metal content (Figure 8). Differences between the samples are also confirmed by the Porod representation (Figure 9) (see Appendix eqs 4 and 5). The intersections yield the values of the tail end constants K_p determined by linear extrapolation for each sample. The value of K_p proportionate to the magnitude of the interfaces of the individual phases tends to increase with increasing the quantity of small-sized rhodium particles in samples. When rhodium particles are intercalated into the kaolinite lamellaes the K_p is increased significantly. Its value is K_p = 58.61 Cps/nm^3 for kaolinite and it increases to 178.67 Cps/nm^3 and 230.31 Cps/nm^3 in the samples containing 0.5 wt % and 1.0 wt % rhodium, respectively. In the case of Rh-montmorillonite samples increasing of the Porod constant may also be observed. The specific surface area (S_p) calculated from the K_p/M_1 is larger for montmorillonite (S_p = 73.45 m^2/g; it has a rough surface), and its value increases if we incorporate polymer (S_p = 93.3 m^2/g) or metal nanoparticles (S_p = 102.49 m^2/g) in the interlamellar space of the clays (see Appendix eq 6). At identical metal content, scattering intensity is increased more in the case of montmorillonite (Figure 8). The value of the correlation length l_c, calculated from K_p, does not change significantly in montmorillonite samples and hardly changes in kaolinite showing the effects of disaggregation in these samples (see Appendix eq 7 and Table 4).

The valence of the rhodium particles on the support surface was examined by XPS analysis. Rh 3d XP spectra of the Rh-montmorillonite (2.0 wt %) and Rh-kaolinite (2.0 wt %) composites are displayed in Figure 10. The broad peaks of Rh3d suggests more than one type of rhodium. Both spectra show the characteristic 3d doublet plus an Mg Auger line in the Rh/montmorillonite sample (at 306.1 eV). The spectra were deconvoluted into two states: Rh^0 and Rh^{3+}. The input parameters were the approximate binding energies of the Rh $3d_{5/2}$ peaks, the energy difference between the Rh $3d_{3/2}$ and Rh $3d_{5/2}$ peaks (4.8 eV), and the intensity ratio of the two peaks (2:3). An additional condition was that the full widths of half-maximums should be equal for all peaks.

The binding energies of the doublet for $Rh3d_{5/2}$ and $Rh3d_{3/2}$ (306.6 and 311.4 eV) are characteristic of Rh^0. Moreover, the peaks at 308.8 and 313.6 eV are observed. These peaks at higher binding energy may be accounted for by the oxidized state of the rhodium. Because the peak areas are proportional to the number of the given

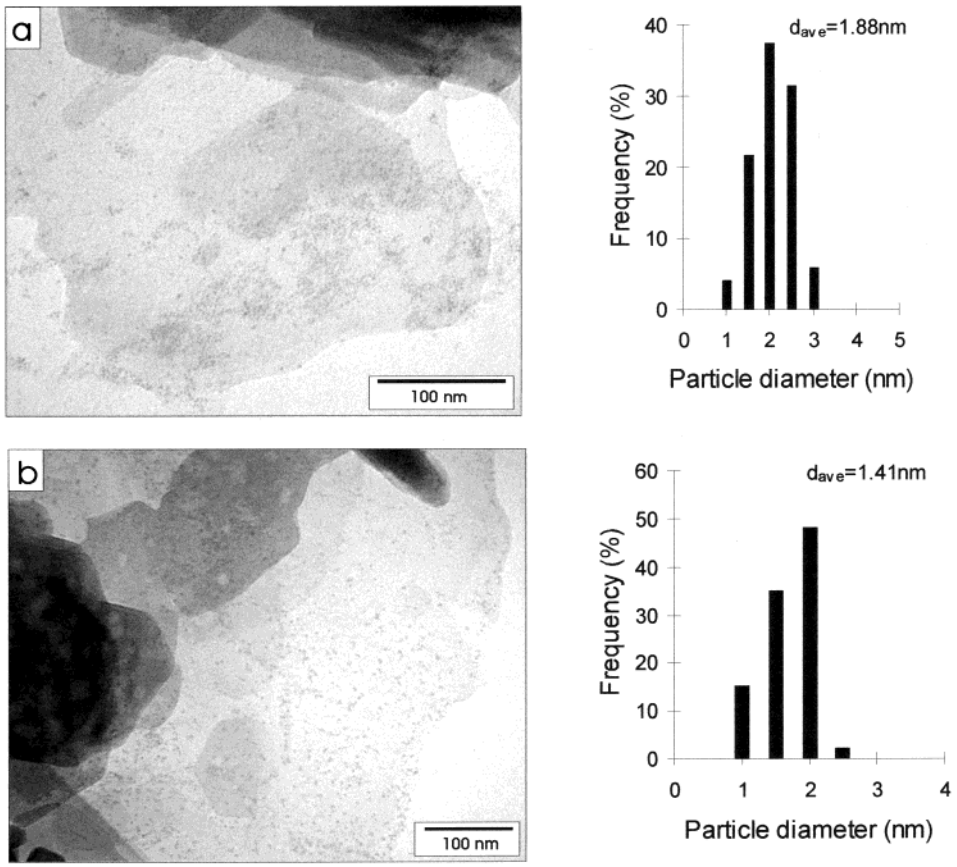

Figure 7. TEM image and particle size distribution of high-molecular-weight PDDACl-protected Rh^0-kaolinite (1 wt % Rh) (a); Rh^0-kaolinite (0.5 wt % Rh) (b).

Table 4. SAXS Parameters of Clay Minerals and Intercalated Samples

SAXS parameters	montm.	PVPM	RhM (0.5 wt %)	RhM (1.0 wt %)	kaolinite	PVPK	RhK (0.5 wt %)	RhK (1.0 wt %)
D_s	2.909	3.08	3.075	3.087	2.417	2.464	2.552	2.521
K_p (Cps/nm^3)	222.26	296.39	478.9	422.54	58.61	66.89	178.67	230.31
M_1 (Cps/nm^2)	3600.24	3176.53	3707.928	3296.97	1388.827	1552.148	2318.087	1941.67
K_p/M_1	0.0617	0.0933	0.1292	0.1282	0.0422	0.0431	0.0771	0.1186
S/V (nm^2/nm^3)	0.05	0.089	0.129	0.125	0.036	0.0423	0.0472	0.116

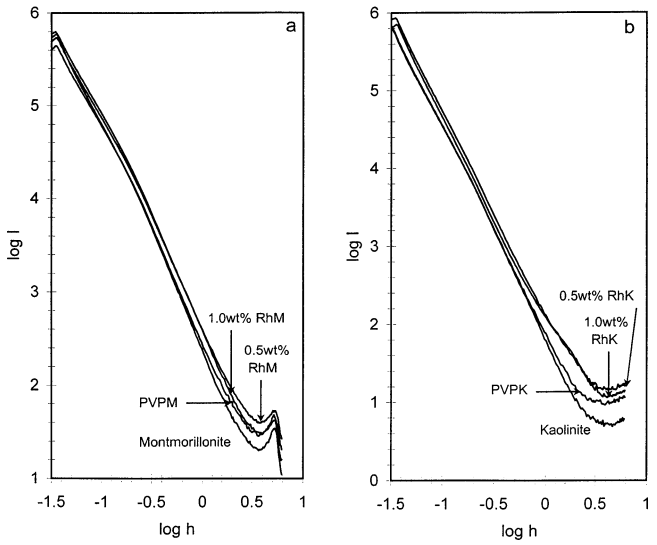

Figure 8. SAXS curves of Rh^0-montmorillonite (a) and Rh^0-kaolinite samples (b).

type of atoms at or near the surface, the deconvolution may help determine the Rh^0/Rh^{3+} ratio. Thus, in the case of montmorillonite-supported Rh this ratio was around 2. This value was cca. 1.8 for the kaolinite-supported sample. So—taking into account the precision of this method—we can say that the Rh^0/Rh^{3+} ratio was the same in both cases. These results indicate that Rh^{3+} was reduced to Rh^0 and that the surface of rhodium particles was partially oxidized in air to Rh_2O_3. The reason might be that ultrafine rhodium particles are very active, which is a common feature for nanometer-sized metal particles, and the Rh^{3+}-ions were not fully reduced by sodium borohydride at the preparation of nanoparticles with the various reduction processes. The possibility that the presence of Rh^{3+} on the surface is a consequence of the metal−support interaction cannot be excluded either.

Conclusion

Rhodium nanosols, furthermore rhodium/montmorillonite and rhodium/kaolinite composites, were prepared in aqueous medium. The particles formed were stabilized with polymers and the lamellae of clay minerals. The effect of the charge, the molecular mass, and the concentration of polymers on particle size was studied using polivinylpyrrolidone, poly(diallyldimethylammonium chloride), and poly(sodium 4-styrenesulfonate).

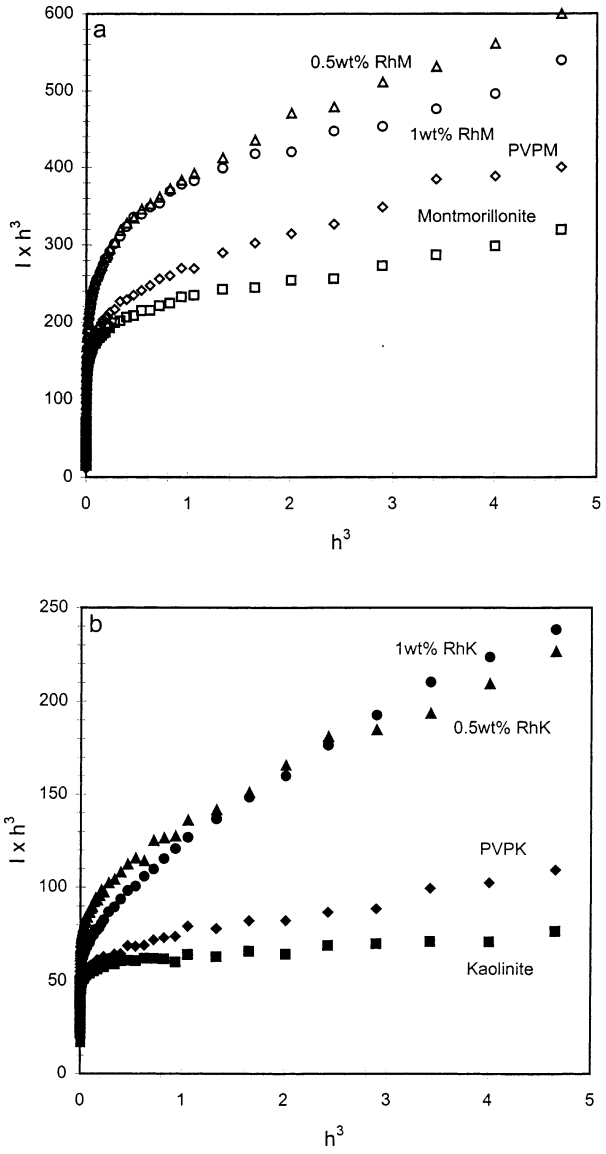

Figure 9. Porod representation of the SAXS curves: Rh^0-montmorillonite (a) and Rh^0-kaolinite samples (b).

Metal content was varied between 0.5 and 2.0 wt %. Interlamellar incorporation of nanoparticles was confirmed by X-ray diffraction in every case, with the exception of the Rh/montmorillonite and the Rh/PSSN/montmorillonite systems. In the case of montmorillonite, intercalation of rhodium nanoparticles was promoted by polymers, and the intercalation of polymers was significantly reduced (7−17%) in the absence of nanoparticles. In the case of kaolinite, too, there is a vast difference between the structure of the mineral supplemented with only polymer or only metal and that of the three-component system (polymer/metal/kaolinite) which displays a new reflection at about 2.7−2.8 nm in a proportion of 21−26%. It was established by transmission electron microscopy that, depending on the stabilization method employed and the concentration of the precursor Rh ions, average particle size falls in the range of 1−3 nm on montmorillonite and 1−2 nm on kaolinite, because adhesion forces operating between kaolinite lamellae are stronger. SAXS experiments are also suitable for the detection of polymer chains and rhodium nanoparticles on the surface of supports. Changes in structural parameters characterize the internal structural changes resulting from the intercalation of rhodium particles.

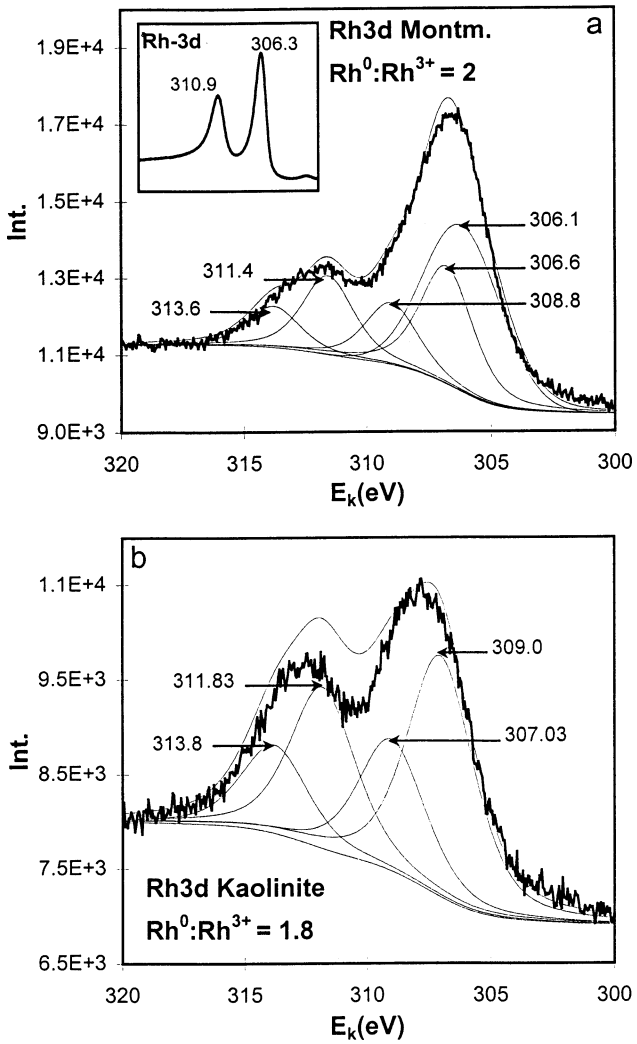

Figure 10. XPS Rh *3d* spectra of Rh^0-montmorillonite (a) and Rh^0-kaolinite samples (b).

XPS analysis indicated the presence of two types of rhodium on the surface: Rh^0 and Rh^{3+}.

Acknowledgment. We thank the Hungarian National Scientific Research Foundation for their financial support (OTKA T034430 and M036688).

Appendix

Calculation Methods for Small-Angle X-ray Scattering by Disperse Systems. When X-rays are scattered by colloidal particles due to differences in electron density caused by inhomogeneities, the intensity of scattered radiation is a function of the angle of scattering (θ) and the scattering vector (h):[52−55]

$$I(h) = \eta^2(0)V\int_0^\infty 4\pi r^2\gamma_0(r)\frac{\sin hr}{hr}\,dr \qquad (1)$$

where V is the volume of the system in which X-rays

(52) Glatter, O.; Kratky, O. *Small-Angle X-ray Scattering*; Academic Press: New York, 1982.
(53) Guinier, A.; Fournet, G. *Small-Angle Scattering of X-rays*; Wiley: New York, 1955.

are scattered by electrons. In the above equation the value of $\eta^2(0)$ can be defined in the following way:[52−55]

$$\eta^2(0) = \frac{1}{V}\int_0^\infty (\rho_e(r) - \rho_e)^2 \, d^3r \tag{2}$$

where $\rho_e(r)$ is the local electron density at a given point (r) and ρ_e is the average electron density. When the concept of electron density fluctuation is introduced: $\eta(r) = \rho_e(r) - \rho_e$, then the correlation function in eq 1 can be given as

$$\gamma_0(r) = \frac{\eta^2(r)}{\eta^2(0)} \tag{3}$$

The correlation function contains significant information on the geometry and structural arrangement of the scattering particles.

The following relationship holds for the tailing region of the scattering function, where $hR > 1$ (the so-called Porod-range):[55−60]

$$I(h) = \eta^2(0) 2\pi \frac{S}{h^4} \tag{4}$$

where S is the surface area of the particles. The relative specific surface area of the particles (relative to unit volume V) is[54−56]

$$\frac{S}{V} = \pi \frac{\lim_{h\to\infty} I(h)h^4}{Q} = \pi \frac{K_p}{Q} \tag{5}$$

where K_p is the tail end constant.

The specific surface area is

$$S_p = \frac{S/V \times 10^3}{d} \tag{6}$$

where d/g cm^{-3} is the density of the disperse system.

Correlation length can also be calculated directly from the scattering function, in case if the following integrations are known:[57−60]

$$l_c = \pi \frac{\int_0^\infty I(h) h \, dh}{Q} \tag{7}$$

From the middle section of the scattering curve the fractal dimension of the particles can be determined;[57] if the scattering curve is linear in the relatively wide range of h: $\log I(h) = p \log h$. From the value of the tangent p, the surface fractal D_s is calculated by the relationship $D_s = p + 5$, the value of which has to fall within the range of $2 \le D_s \le 3$.

CM0310667

(54) Porod, G. *Kolloid-Zeitschrift.* **1951**, *124*, 83.
(55) Kratky, O. *Angew Chem.* **1960**, *72*, 467.
(56) Kratky, O.; Laggner, P. *Encycl. Phys. Sci. Technol.* **1987**, *14*, 693.
(57) Schmidt, P. W.; Avnir, D.; Levy, D.; Hohr, A. *J. Chem. Phys.* **1991**, *94*, 1474.
(58) Hurd, J. A.; Schaefer, D. W.; Martin, J. E. *Phys. Rev.* **1987**, *5*, 2361.
(59) Zipper, P.; Janosi, A.; Wrentschur, E.; Abuja, P. A. *J. Appl. Crystallogr.* **1991**, *24*, 702.
(60) Kriechbaum, M.; Degovics, G.; Tritthardt, J. *Prog. Colloid Polym. Sci.* **1989**, *79*, 101.